J Therm Spray Tech (2022) 31:991–999
https://doi.org/10.1007/s11666-021-01295-8

PEER REVIEWED

Microstructure and Properties of Laser-cladded $Fe_{50}Mn_{30}Co_{10}Cr_{10}$ High Entropy Alloy Coatings

Hao Liu[1] · Xianfen Li[1,2] · Peng Hua[1,2] · Kuijing Song[1,2] · Peng Teng[1] · Wei Zhou[1,3]

Submitted: 9 May 2021 / in revised form: 15 November 2021 / Accepted: 29 November 2021 / Published online: 3 January 2022

Abstract $Fe_{50}Mn_{30}Co_{10}Cr_{10}$ high-entropy alloys were prepared by laser cladding technology. The microstructure and phase structure of the cladding layer were analyzed. The effects of laser cladding parameters on mechanical property of the cladding layer were studied. The results show that, the $Fe_{50}Mn_{30}Co_{10}Cr_{10}$ high entropy alloy cladding layer is composed of FCC structure and HCP structure, BCC structure was also observed in the layer. There are fine equiaxed grains at the top of the cladding layer while columnar grains near the fusion zone. The maximum hardness of cladding layer is 292.9 HV under the laser cladding parameter of 200 W and 5 mm/s. The maximum tensile strength of the substrate with cladding layer is 692.4 MPa, and the maximum elongation is 21.3%. The fracture mode of cladding layer is ductile fracture. Adhesive wear and abrasive wear are both observed at surface of the cladding layer after wear testing. The best wear resistance is obtained at cladding parameter of 200 W, 7 mm/s with the weight loss of 0.0215g and friction coefficient of 0.6294. The results provide a certain support for the preparation process and microstructure, properties analysis of $Fe_{50}Mn_{30}Co_{10}Cr_{10}$ high entropy alloy.

Keywords high entropy alloy · laser cladding · microstructure · tensile properties · wear resistance

Introduction

As a new metal material, high-entropy alloy has been widely studied in recent years. Because of its four core effects, named "High-entropy effect", "Severe lattice-distortion effect", "Sluggish diffusion effect" and "Cocktail effect" (Ref 1, 2), it obtains excellent properties such as high strength (Ref 7), high hardness (Ref 4), high wear resistance (Ref 5), high corrosion resistance (Ref 6) and high thermal stability (Ref 7-10).

Traditionally, high-entropy alloys are composed of five or more major alloy elements, and the atomic fraction of each element is between 5 and 35 % (Ref 11). And only a single solid solution phase, such as face center cubic (FCC) structure, will be found in this kind of traditional high-entropy alloy. In recent years, with the deepening of research, the concept of high-entropy alloy has been developed. The main alloy elements can be four or more alloy elements, and the phase structure can also be dual-phase or multi-phase (Ref 12, 13). This kind of high-entropy alloy has been accepted and studied by more and more scholars. For example, Huang et al. (Ref 14) prepared CoCrFeNi high-entropy alloy by

This article is part of a special topical focus in the Journal of Thermal Spray Technology on High Entropy Alloy and Bulk Metallic Glass Coatings. The issue was organized by Dr. Andrew S.M. Ang, Swinburne University of Technology; Prof. B.S. Murty, Indian Institute of Technology Hyderabad; Distinguished Prof. Jien-Wei Yeh, National Tsing Hua University; Prof. Paul Munroe, University of New South Wales; Distinguished Prof. Christopher C. Berndt, Swinburne University of Technology. The issue organizers were mentored by Emeritus Prof. S. Ranganathan, Indian Institute of Sciences.

✉ Xianfen Li
lxfytt@163.com

[1] School of Materials Science and Engineering, Hefei University of Technology, Hefei 230009, People's Republic of China

[2] Engineering Research Center of High Performance Copper Alloy Materials and Processing, Ministry of Education, Hefei, China

[3] School of Mechanical and Aerospace Engineering, Nanyang Technological University, 50 Nanyang Avenue, Singapore 639798, Singapore

vacuum melting, and studied the effect of carbon addition on its microstructure and properties. It was found that with the addition of carbon, the degree of solution strengthening of $CoCrFeNiC_X$ high-entropy alloy increased. A little carbides precipitated, which led to the improvement of hardness and strength of the alloy, as well as the improvement of wear resistance. Nutor et al. (Ref 15) designed a non-equiatomic high-entropy alloy $Fe_{50}Mn_{27}Ni_{10}Cr_{13}$, which reduced the amount of Co compared with the traditional FeMnCoCrNi high entropy alloy. It not only has good mechanical properties and corrosion resistance, but also improves the economic effect due to the reduction of Co element.

Li et al. (Ref 16) used a method called "metastable engineering" to design a high-entropy alloy with high strength and high toughness. By controlling the content of Mn in $Fe_{80-x}Mn_xCo_{10}Cr_{10}$, it was found that when the atomic percentage of Mn is 30%, FCC structure and HCP (hexagonal close-packed) structure appear simultaneously in this high-entropy alloy. The dual-phase high-entropy alloy has TWIP (twinning induced plasticity) and TRIP (transformation induced plasticity), which improve its strength without losing its toughness.

The preparation of high-entropy alloy coatings by laser cladding has become a research hot spot in recent years (Ref 17). Compared with traditional methods for preparing high-entropy alloys such as vacuum melting, laser cladding has the advantages such as small heat-affected zone, compact structure, better mechanical properties (Ref 18-21), less pollution, and higher economic benefit (Ref 22). At present, there have been some researches on the traditional high-entropy alloy coatings prepared by laser cladding technology, as well as the mechanical properties and microstructure characteristics of high-entropy alloy coatings with different elements (Ref 23-25). However, there are few studies on the preparation of non-equivalent four elements high-entropy alloys by laser cladding.

In this study, the laser cladding technology will be used to prepare Fe50Mn30Co10Cr10 high-entropy alloy on the 304L substrate. It can play the role of surface modification of 304L steel, so as to improve the surface properties of the substrate. At the same time, when the substrate is seriously worn, the coatings can also re-fabricate or repair it. The focus will be on the effect of laser cladding process parameters on the microstructure and properties of the $Fe_{50}Mn_{30}Co_{10}Cr_{10}$ high-entropy alloy coating, which is expected to provide some help to the preparation technology of high-entropy alloy.

Experimental Materials and Methods

In order to obtain high-purity high-entropy alloy powders, Fe, Mn, Co, and Cr powders with purity higher than 99.5% were smelted into high-entropy alloy at the atomic ratio of 5:3:1:1. Then it was atomized into $Fe_{50}Mn_{30}Co_{10}Cr_{10}$ high-entropy alloy powder, the particle size of the high-entropy alloy powder is about 25 μm. 304L stainless steel with a size of 150 mm × 200 mm × 14 mm was used as the substrate. The surface of the substrate was polished with sandpaper, and then cleaned with alcohol and acetone solution. Laser cladding test was carried out by preset coating method. A certain amount of high-entropy alloy powder was mixed with alcohol to form a viscous shape and scraped on the substrate with a scraper. The thickness of the preset coating powder layer is approximately 250 μm which was dried at 100 °C for 1 hour. The laser cladding experiment was carried out with LWS-1000 Nd: YAG laser, the laser power is 200 W, 250 W, scanning speed is 3 mm/s, 5 mm/s, and 7 mm/s, respectively. The diameter of laser spot is 1 mm, pulse width is 2 ms, pulsed frequency is 25 Hz, and overlap rate is 50%. In the process of laser cladding, 10 L/min of Ar was introduced as a protective gas. After laser cladding, the sample were cut into blocks of 10 mm × 10 mm × 14 mm and a cylinder with a diameter of 4.8 mm.

The morphology and microstructures of the sample were observed by optical microscope (OM, HT630CN) and scanning electron microscopy (SEM, Gmini-500), 50% aqua regia solution was used for the sample corrosion. Energy dispersive x-ray spectroscopy (EDS, Oxford Inca Energy350) was used to analyze element distribution. X-ray diffraction (XRD, D/MAX2500V) was used to analyze the phase structure (Fig. 1). Micro-hardness of the cladding layer was measured by Warnway VTS401. The measurement was carried out from the uppermost direction of the cladding layer to the direction of the substrate with a load of 50 g and a holding time of 15 s. The double-sided cladding 304L was used for tensile test on CMT5150 Universal tester with a constant displacement rate of 1 mm/min. The tensile specimens were cut as shown in Fig. 2. For the wear resistance test, the friction pair made of quenched

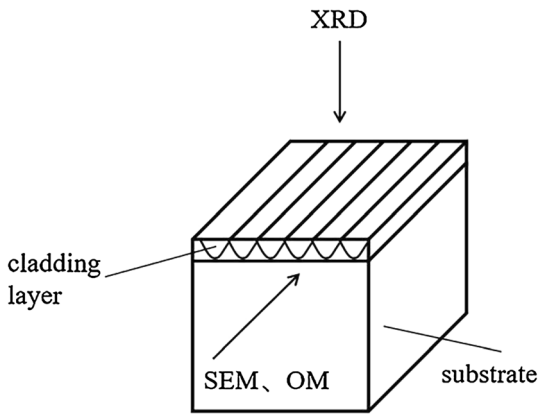

Fig. 1 Schematic diagram of test direction

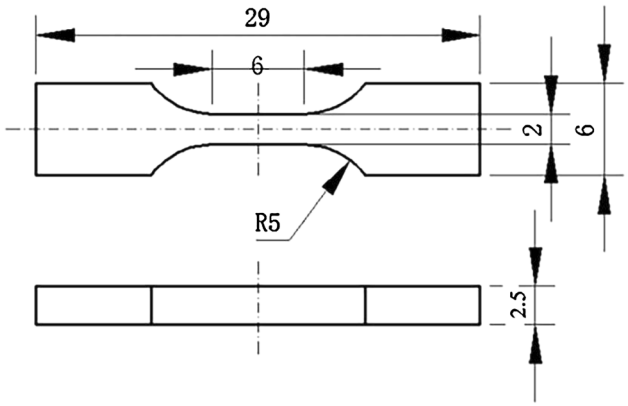

Fig. 2 Schematic diagram of tensile specimen

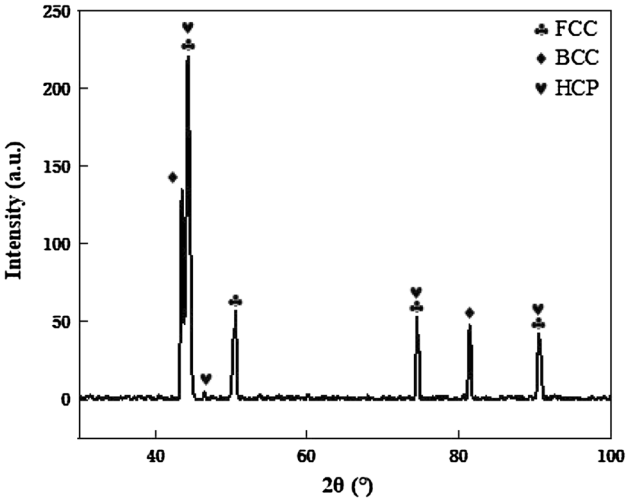

Fig. 3 XRD diffraction pattern of laser cladding coating

45 steel was adopted. The rotating speed is 100 R/min, the load is 20 N, and the duration time is 30 min. The test was carried out under dry friction conditions.

Results and Analysis

Microstructure and Phase Structure of Laser Cladding Coating

The XRD analysis of laser cladding coating is shown in Fig. 3. The $Fe_{50}Mn_{30}Co_{10}Cr_{10}$ high-entropy alloy cladding layer is mainly composed of FCC and HCP structure, BCC structure can also be observed. Under the "high-entropy effect", the formation of complex inter-metallic compounds is inhibited, so that high-entropy alloys always appear to form solid solution structure, such as FCC and HCP. According to research (Ref 16), the HCP structure is a metastable structure in the high-entropy alloy, and the Mn element can regulate its content, so that it has TWIP and TRIP effects. It can not be ignored that the BCC structure also appears in the XRD results. This may be the non-equilibrium structure formed under the high entropy effect and rapid cooling rate of laser cladding process (Ref 27, 28). At the same time, a large number of Cr elements will also stabilize the BCC structure.

Figure 4 shows the Microstructure of $Fe_{50}Mn_{30}Co_{10}Cr_{10}$ high-entropy alloy cladding layer under an optical microscope. In the laser cladding process, the laser melts and solidifies the preset powder and the substrate together to form a cladding layer. With the laser power increasing, the thickness of the cladding layer has been significantly

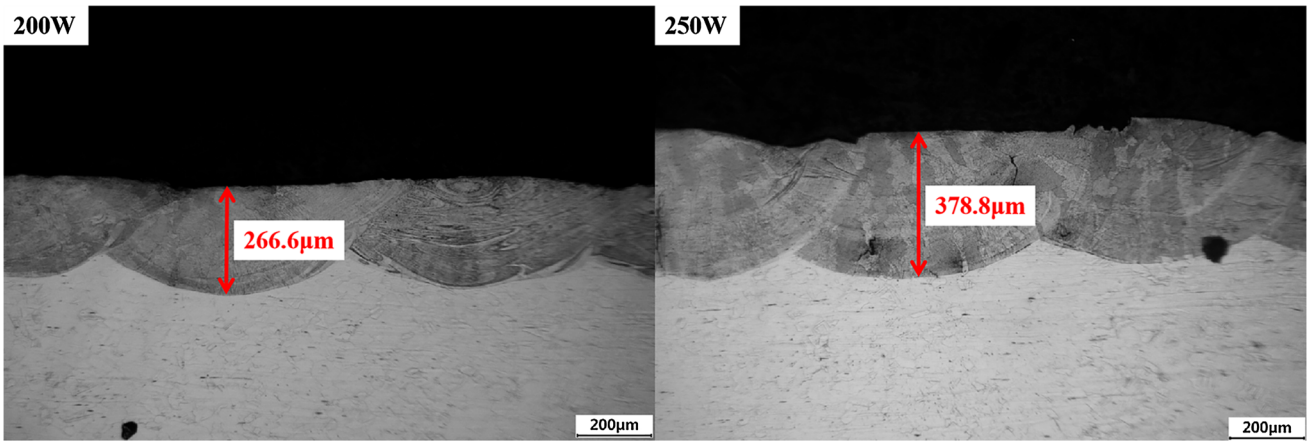

Fig. 4 Cladding thickness under different laser power (a) 200W. (b) 250W

improved, from 266.6 to 378.8 μm, which is about 1.4 times. When the laser power is 250 W, the thickness of the laser cladding coating has far exceeded the thickness of the preset powder. Since the preset powder thickness is constant, the increase of cladding layer thickness means the increase of penetration of cladding layer. The larger penetration shows that more substrate is melted into the cladding layer in the process of laser cladding, which will result in a great change in the composition of the high-entropy alloy cladding layer. Figure 5 shows the microstructure of the laser cladding coating at a higher magnification. The laser cladding coating and the substrate have a distinct layer without an obvious transition area. The microstructure of laser cladding coating is relatively dense with no obvious defects under the laser cladding parameter of 200W (as shown in Figs. 4a and 5).

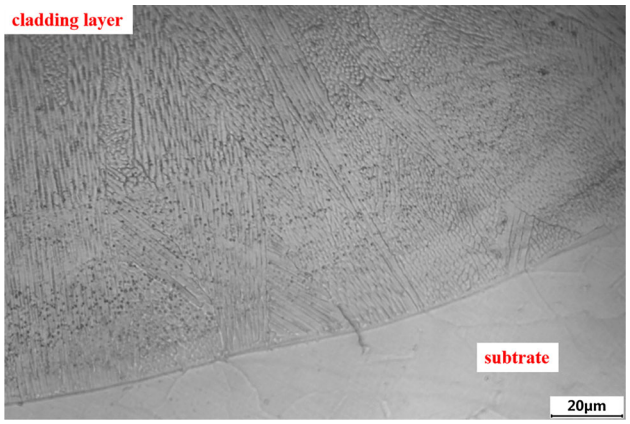

Fig. 5 Metallographic diagram of laser cladding coating at 200W

Figure 6 shows the SEM of the $Fe_{50}Mn_{30}Co_{10}Cr_{10}$ high-entropy alloy cladding layer. The top of the laser cladding coating is mainly composed of fine equiaxed crystals, while the bottom is composed of columnar dendritic structures with different directions. In the laser cladding process, the instantaneous heat input is large, and the cooling speed is fast. Under the impact of the laser, the preset powder and the substrate are melted at a high temperature to form a structure similar to a welding molten pool. During cooling, the crystal grains grow along the direction of heat flow, that is, perpendicular to the isotherm, thereby forming columnar crystals. However, the top of the cladding layer rapidly nucleated under the influence of a faster cooling rate to form fine equiaxed crystals. The size of fine equiaxed crystals was only a few microns.

The EDS scanning results of the laser cladding coating are shown in the Fig. 7 and Table 1. The result showed that Fe, Mn, Co and Cr all appeared inside the cladding layer, and the distribution of each element was uniform, indicating that the composition of the cladding layer was uniform. Among them, the atomic ratio of Fe element has increased to a higher extent, while the atomic ratio of Mn element has decreased to a greater extent. The reason for this phenomenon is that part of the 304L substrate is melted by the laser, which leads to an increase in Fe content in the cladding layer. The second reason is that Mn has a higher metal vapor pressure and a certain tendency of oxidation in

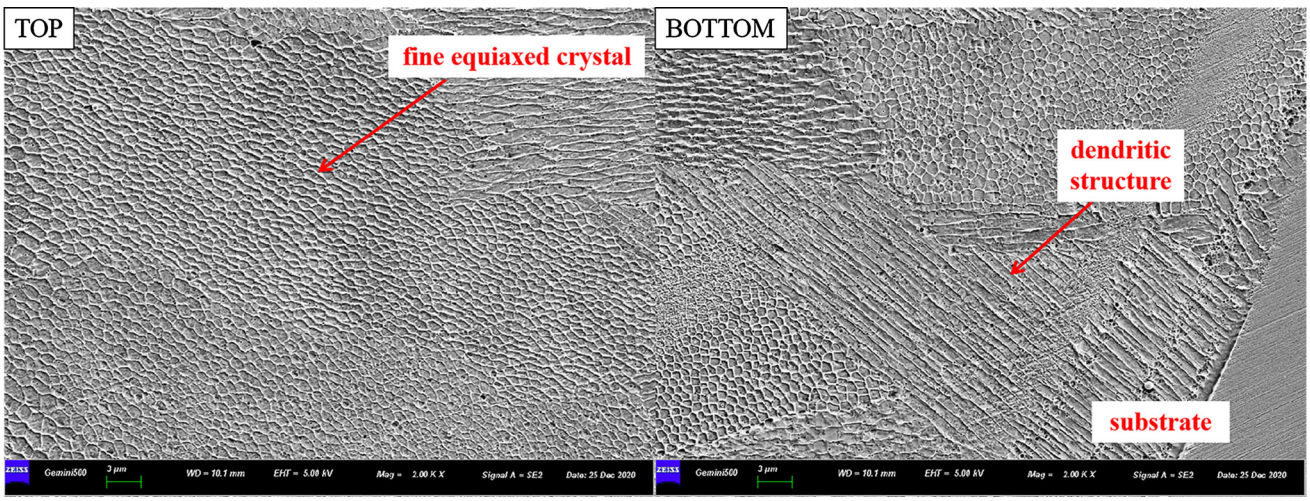

Fig. 6 SEM of laser cladding coating

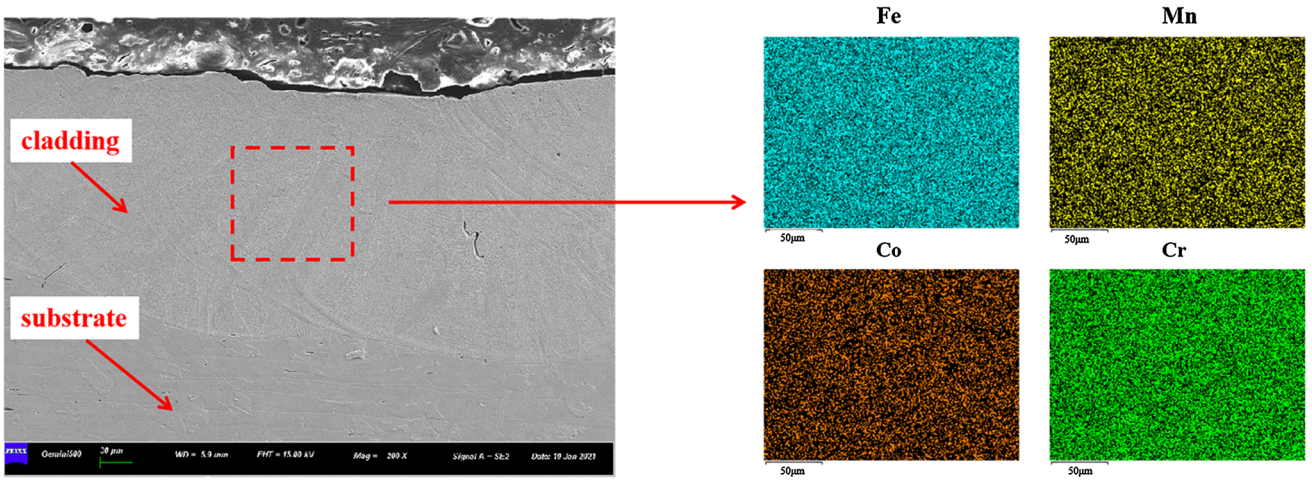

Fig. 7 EDS analysis of laser cladding coating

Table 1 EDS result of laser cladding coating

Elements	Fe	Mn	Co	Cr
Chemical composition (at.%)	68.4	11.3	6.1	14.2

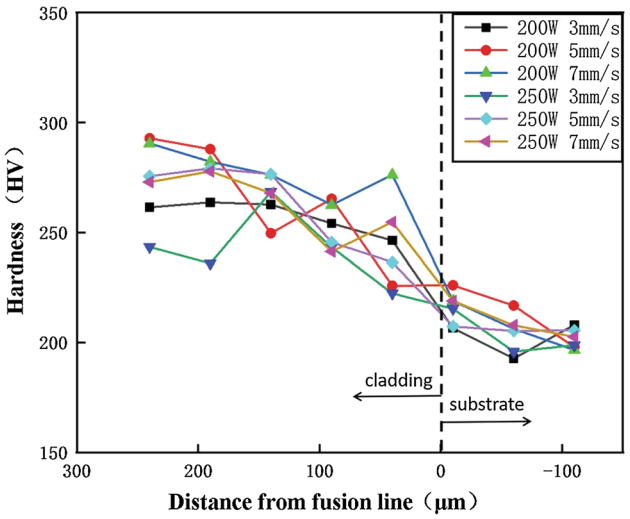

Fig. 8 Hardness of laser cladding coating under different process parameters

laser cladding process (Ref 26), which ultimately leads to a decrease in the Mn content.

Mechanical Properties of Laser Cladding Coating

Figure 8 shows the micro-hardness of the $Fe_{50}Mn_{30}Co_{10}Cr_{10}$ high-entropy alloy cladding layer under different process parameters. The hardness is measured from the surface of the laser cladding coating down to the substrate. The maximum hardness value is obtained with laser power of 200W, scanning speed of 5 mm/s, which is 292.9 HV. While the smallest hardness value is obtained with laser power of 250 W, scanning speed of 3 mm/s, which is 222.3 HV. Although the overall hardness distribution of the laser cladding coating is relatively uniform, the hardness near the top of the cladding layer is slightly higher than the hardness near the fusion zone. Combined with the analysis of the microstructure of the cladding layer in the previous article, it can be seen that the increase of hardness is due to the rapid cooling and solidification characteristics of laser cladding. The fine equiaxed crystals are formed on the top of the cladding layer, resulting in fine-grain strengthened effect. However, the grains near the fusion zone gradually become thicker to form columnar dendrites, and the hardness here is lower due to the effect of substrate dilution. Comparing the hardness under different process parameters, we found that when the laser power is low and the scanning speed is high, the overall hardness value of the cladding layer is higher due to the small heat input, and the cladding layer cools faster resulting in a smaller crystal grain size. The finer grains allow the whole cladding layer to gain higher hardness.

Tensile tests were carried on 304L substrate samples with $Fe_{50}Mn_{30}Co_{10}Cr_{10}$ high-entropy alloy cladding layer under different process parameters. Figure 9 shows the SEM fracture appearance after tensile test. The cladding layer and the substrate can be clearly distinguished. The necking at the fracture of the substrate is not clear, and the fracture goes along a plane at 45° to the surface of the substrate, which is a typical ductile fracture. Smaller dimples appear in the cladding layer, and the fracture mode is also ductile fracture. Li et al. (Ref 16) also pointed out that the metastable HCP structure in the $Fe_{50}Mn_{30}Co_{10}Cr_{10}$ high-entropy alloy will transform to the FCC structure under the action of stress, thereby inducing the TWIP and

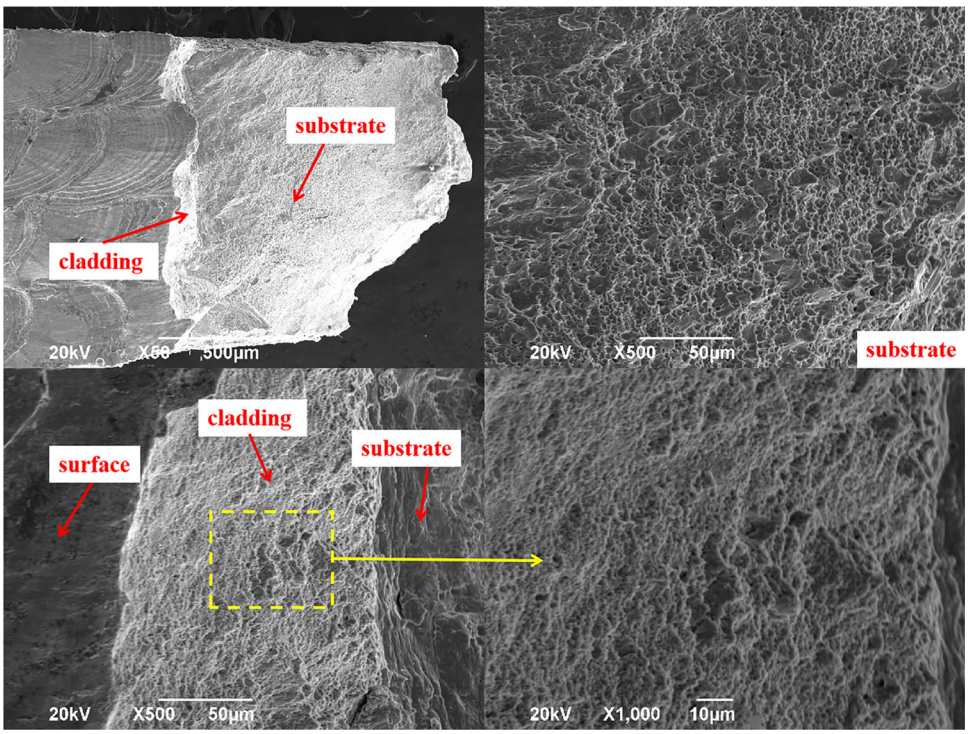

Fig. 9 Fracture morphology of 304L with cladding layer

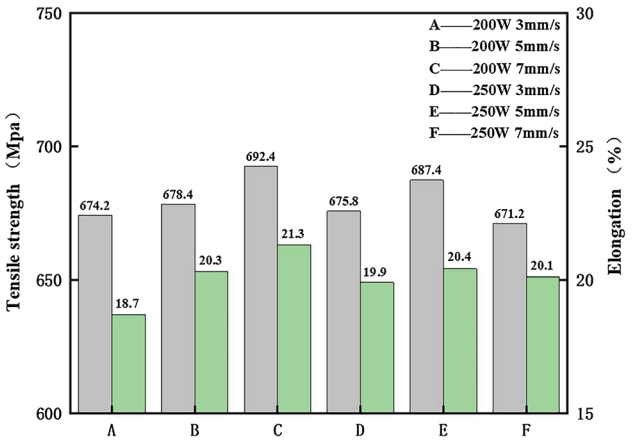

Fig. 10 Tensile properties of double clad specimens under different process parameters

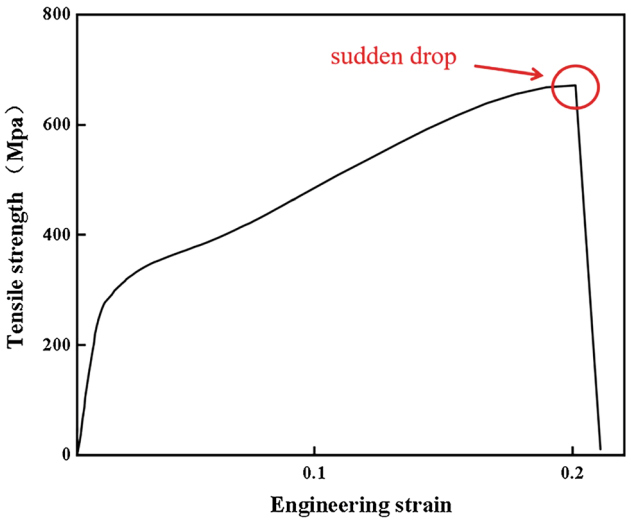

Fig. 11 The stress-strain curve of 304L with cladding layer at 200W 7 mm/s

TRIP and making the $Fe_{50}Mn_{30}Co_{10}Cr_{10}$ high-entropy alloy have higher toughness. A large number of elongated dimples were observed from the substrate, indicating a typical ductile fracture. At the same time, signs of tearing can be observed.

Figure 10 shows the maximum tensile strength and elongation under different process parameters. The maximum tensile strength of 692.4 MPa and elongation of 21.3% were obtained with the laser power of 200 W and scanning speed of 7 mm/s. From an overall point of view, after double-sided cladding under different process parameters, the maximum tensile strength and elongation is similar, which indicates that all the cladding layer obtained under these process parameters are well formed. Figure 11 shows the stress-strain curve of a tensile specimen with double-sided cladding. When the maximum tensile strength is reached, the stress-strain curve has a "sudden drop". In the tensile test, with the load increasing, once the load exceeds the maximum tensile strength of the cladding layer, cracks will appear in the cladding zone. As the load continues to increase, cracks will rapidly expand from the cladding zone to the substrate causing the entire sample to fracture.

Table 2 Wear test result of laser cladding coatings

	Weight before test (g)	Weight after test (g)	Weight loss (g)	Friction coefficient
Substrate	1.7538	1.7285	0.0253	0.8169
	1.7536	1.7262	0.0277	0.7238
200W 3 mm/s	1.7477	1.7212	0.0265	0.6894
200W 5 mm/s	1.7544	1.7311	0.0233	0.6657
200W 7 mm/s	1.7500	1.7285	0.0215	0.6294
250W 3 mm/s	1.7502	1.7218	0.0284	0.6948
250W 5 mm/s	1.7533	1.7295	0.0238	0.6665
250W 7 mm/s	1.7490	1.7262	0.0228	0.6345

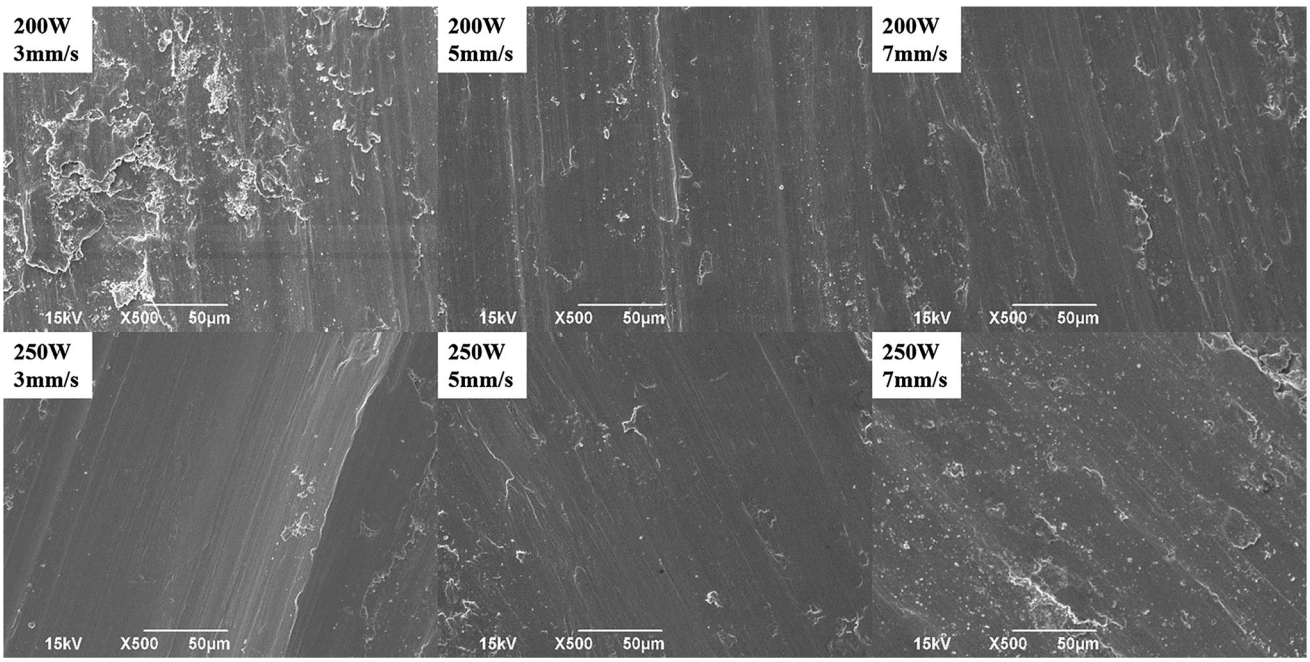

Fig. 12 The worn surfaces of the cladding layer under different laser cladding parameters

Wear Resistance

The wear test is carried out under the condition of dry friction, accompanied with oxidation and weight loss of cladding layer (Ref 29). In this paper, the emphasis is to discuss the result of wear resistance through appearance, weight loss and friction coefficient. Table 2 shows the weight loss and average wear friction coefficient of the cladding layers. The lowest average weight loss of 0.0215g and average friction coefficient of 0.6294 are obtained at laser cladding parameter of 200W, 7 mm/s, which shows the cladding layer gets the best wear resistance. The worn surfaces of the cladding layer under different laser cladding parameters are shown in the Fig. 12. It can be observed that furrows with different depths were produced in the test, showing that the type of wear is abrasive wear. At the same time, the adhesion between the cladding layer and the friction pair occurred resulting in the peeling off of the cladding surface, showing that the type of wear is adhesive wear. Therefore, the wear type of $Fe_{50}Mn_{30}Co_{10}Cr_{10}$ high-entropy alloy cladding layer is a composite wear form of adhesive wear and abrasive wear. When the laser scanning speed is 3mm/s, the sample hardness is lower, it can be observed that the surface of the cladding layer is seriously worn, the peeling off of the cladding surface is serious, and the furrow on the surface of the cladding layer is deep with large plastic deformation. According to Archard's law, the wear resistance of materials is directly proportional to Vickers hardness. The hardness obtained at laser cladding parameter of 200W, 7 mm/s is higher, so it has strong resistance to plastic deformation and inhibits the wear of the grinding pair on

the cladding surface. The higher hardness value and the best wear resistance are obtained under the same parameter sample cladded at laser cladding parameter of 200W, 7 mm/s.

Conclusions

The $Fe_{50}Mn_{30}Co_{10}Cr_{10}$ high-entropy alloy was prepared by laser cladding. The microstructure and the properties of the $Fe_{50}Mn_{30}Co_{10}Cr_{10}$ high-entropy alloy cladding layer were investigated, following Conclusions are summarized:

1. The cladding layer of $Fe_{50}Mn_{30}Co_{10}Cr_{10}$ high-entropy alloy is mainly composed of FCC structure and HCP structure, BCC structure also can be observed. The top of the cladding layer is fine equiaxed crystals, and the bottom is composed of columnar crystals that grow parallel to the direction of heat flow.
2. The maximum cladded layer hardness value is 292.9 HV. The wear type of $Fe_{50}Mn_{30}Co_{10}Cr_{10}$ high-entropy alloy cladding layer is a composite wear form of adhesive wear and abrasive wear. The best wear resistance of weight loss of 0.0215g and friction coefficient of 0.6294 is obtained with the specimen cladded at laser cladding parameter of 200W, 7 mm/s.
3. $Fe_{50}Mn_{30}Co_{10}Cr_{10}$ high-entropy alloy cladding layer has good tensile properties, and the fracture mode is ductile fracture. The maximum tensile strength and maximum elongation of the substrate with cladding layer is 692.4 MPa and 21.3%.

References

1. D.B. Miracle and O.N. Senkov, A Critical Review of High Entropy Alloys and Related Concepts, *Acta Mater.*, 2017, **122**(1), p 448.
2. Y. Zhang, T.T. Zuo, Z. Tang, M.C. Gao, K.A. Dahmen, P.K. Liaw and Z.P. Lu, Microstructures and Properties of High-Entropy Alloys, *Prog. Mater. Sci.*, 2014, **61**, p 1–93.
3. Y.P. Lu, X.Z. Gao, L. Jiang, Z.N. Chen, T.M. Wang, J.C. Jie, H.J. Kang, Y.B. Zhang, S. Guo, H.H. Ruan, Y.H. Zhao, Z.Q. Cao and T.J. Li, Directly Cast Bulk Eutectic and Near-Eutectic High Entropy Alloys with Balanced Strength and Ductility in a Wide Temperature Range, *Acta Mater.*, 2017, **124**, p 143–150.
4. M. L. Wang, H. Z. Cui, Y. Q. Zhao, C. M. Wang, N. Wei, Y. Zhao, X. Zhang, Q. Song, A Simple Strategy for Fabrication of an FCC-Based Complex Concentrated Alloy Coating with Hierarchical Nanoprecipitates and Enhanced Mechanical Properties, *Mater. Des.,*2019, **180**.
5. M. L. Wang, Y. P. Lu, G. J. Zhang, H. Z. Cui, D. F. Xu, N. Wei, T. J. Li, A Novel High-Entropy Alloy Composite Coating with Core-Shell Structures Prepared by Plasma Cladding, *Vacuum.*, 2021, **184**.
6. M.L. Wang, Y.P. Lu, G.J. Zhang, H.Z. Cui, D.F. Xu, N. Wei and T.J. Li, Effect of Plasma Remelting on Microstructure and Properties of a CoCrCuNiAl0.5 High-Entropy Alloy Prepared by Spark Plasma Sintering, *J. Mater. Sci.*, 2021, **56**, p 5878–5898.
7. M.H. Chuang, M.H. Tsai, W.R. Wang, S.J. Lin and J.W. Yeh, Microstructure and Wear Behavior of AlxCo1.5CrFeNi1.5Tiy High-Entropy Alloys, *Acta Mater.*, 2011, **59**(16), p 6308–6317.
8. B. Schuh, F. Mendez-Martin, B. Völker, E.P. George, H. Clemens, R. Pippan and A. Hohenwarter, Mechanical Properties, Microstructure and Thermal Stability of a Nanocrystalline CoCrFeMnNi High-Entropy Alloy After Severe Plastic Deformation, *Acta Mater.*, 2015, **96**, p 258–268.
9. W.H. Liu, Z.P. Lu, J.Y. He, J.H. Luan, Z.J. Wang, B. Liu, Y. Liu, M.W. Chen and C.T. Liu, Ductile CoCrFeNiMox High Entropy Alloys Strengthened by Hard Intermetallic Phases, *Acta Mater.*, 2016, **116**, p 332–342.
10. C.P. Lee, C.C. Chang, Y.Y. Chen, J.W. Yeh and H.C. Shih, Effect of the Aluminium Content of AlxCrFe1.5MnNi0.5 High-Entropy Alloys on the Corrosion Behaviour in Aqueous Environments, *Corros. Sci.*, 2008, **50**(7), p 2053–2060.
11. J.W. Yeh, S.K. Chen, S.J. Lin, J.Y. Gan, T.S. Chin, T. Shun, C.H. Tsau and S.Y. Chang, Nanostuctures High-Entropy Alloys with Multiple Principal Elements: Novel Alloy Design Concepts and Outcomes, *Adv Eng Mater*, 2004, **6**(5), p 299–303.
12. M.R. He, S. Wang, K. Jin, H.B. Bei, K. Yasuda, S. Matsumura, K. Higashida and I.M. Robertson, Enhanced Damage Resistance and Novel Defect Structure of CrFeCoNi Under In Situ Electron Irradiation, *Scr. Mater.*, 2016, **125**, p 5–9.
13. J.T. Fan, L.J. Zhang, P.F. Yu, M.D. Zhang, D.J. Liu, Z. Zhou, P. Cui, M.Z. Ma, Q. Jing, G. Li and R.P. Liu, Improved the Microstructure and Mechanical Properties of AlFeCoNi High-Entropy Alloy by Carbon Addition, *Mater. Sci. Eng. A*, 2018, **728**, p 30–39.
14. T.D. Huang, C.L. Zhang, H. Jiang, Y.P. Lu and T.J. Li, Effect of Carbon Addition on the Microstructure and Mechanical Properties of CoCrFeNi High Entropy Alloy, *Sci. China Technol. Sci*, 2018, **61**(1), p 117–123.
15. R.K. Nutor, M. Azeemullah, Q.P. Cao, X.D. Wang, D.X. Zhang and J.Z. Jiang, Microstructure and Properties of a Co-free Fe50Mn27Ni10Cr13 High Entropy Alloy, *J. Alloys Compd.*, 2021, **851**, p 156842.
16. Z.M. Li, K.G. Pradeep, Y. Deng, D. Raabe and C.C. Tasan, Metastable High-Entropy Dual-Phase Alloys Overcome the Strength-Ductility Trade-Off, *Nature*, 2016, **534**(7606), p 227–230.
17. J.L. Liu, H.J. Yu, C.Z. Chen, F. Weng and J.J. Dai, Research and Development Status of Laser Cladding on Magnesium Alloys: A Review, *Opt. Lasers Eng.*, 2017, **93**, p 195–210.
18. L. Dubourg, D. Ursescu, F. Hlawka and A. Cornet, Laser Cladding of MMC Coatings Onaluminium Substrate: Influence of Composition and Microstructure on Mechanical Properties, *Wear*, 2005, **258**(11–12), p 1745–1754.
19. F. Weng, H.J. Yu, C.Z. Chen and J.J. Dai, Microstructures and Wear Properties of Laser Cladding Co–based Composite Coatings on Ti–6Al–4V, *Mater. Des.*, 2015, **80**, p 174–181.
20. H.X. Liu, Q. Xu, C.Q. Wang and X.W. Zhang, Corrosion and Wear Behavior of Ni60CuMoW Coatings Fabricated by Combination of Laser Cladding and Mechanical Vibration Processing, *J. Alloys Compd.*, 2015, **621**, p 357–363.
21. F.Y. Shu, L. Wu, H.Y. Zhao, S.H. Sui, L. Zhou, J. Zhang, W.X. He, P. He and B.S. Xu, Microstructure and High-Temperature Wear Mechanism of Laser Cladded CoCrBFeNiSi High-Entropy Alloy Amorphous Coating, *ACS Mater. Lett.*, 2017, **211**, p 235–238.
22. J.D. Majumdar, R. Galun, B.L. Mordike and I. Manna, Effect of Laser Surface Meltingon Corrosion and Wear Resistance of a

Commercial Magnesium Alloy, *Mater. Sci. Eng. A*, 2003, **361**, p 119–129.
23. X.L. Ji, H. Duan, H. Zhang and J.J. Ma, Slurry Erosion Resistance of Laser Clad NiCoCrFeAl3 High-Entropy Alloy Coatings, *Tribol. Trans.*, 2015, **58**(6), p 1119–1123.
24. W. Wu, L. Jiang, H. Jiang, X.M. Pan, Z.Q. Cao, D.W. Deng, T.M. Wang and T.J. Li, Phase Evolution and Properties of Al2CrFeNiMox High-Entropy Alloys Coatings by Laser Cladding, *J. Therm. Spray Technol.*, 2015, **24**(7), p 1333–1340.
25. C. Ni, Y. Shi, J. Liu and G.Z. Huang, Characterization of Al0.5FeCu0.7NiCoCr High-Entropy Alloy Coating on Aluminum Alloy by Laser Cladding, *Opt. Laser Technol.*, 2018, **105**, p 257–263.
26. J. Y. Aguilar-Hurtado, A. Vargas-Uscategui, K. Paredes-Gil, R. Palma-Hillerns, M. J. Tobar, J. M. Amado, Boron Addition in a Non-equiatomic Fe50Mn30Co10Cr10 Alloy Manufactured by Laser Cladding: Microstructure and Wear Abrasive Resistance, *Appl. Surf. Sci.*, 2020, **515**.
27. Z. Wu, H. Bei, F. Otto, G.M. Pharr and E.P. George, Recovery, Recrystallization, Grain Growth and Phase Stability of a Family of FCC-Structured Multi-Component Equia-tomic Solid Solution Alloys, *Intermetallics*, 2014, **46**, p 131–140.
28. G. Jin, Z. Cai, Y. Guan, X. Cui, Z. Liu, Y. Li, M. Dong and D. Zhang, High Temperature Wear Performance of Laser-Cladded FeNiCoAlCu High-Entropy Alloy Coating, *Appl. Surf. Sci.*, 2018, **445**, p 113–122.
29. J. B. Chen, B. Sun, Y. Y. Ge, X. L. Hu, L. H. Zhang, X. B. Liang, X. C. Zhang, Nb Doping in Laser-Cladded Fe25Co25-Ni25(B0.7Si0.3)25 High Entropy Alloy Coatings: Microstructure Evolution and Wear Behavior, *Surf. Coat. Technol.*2020, **402**.